Optimal energy management of HEVs with hybrid storage system

Emmanuel Vinot, Rochdi Trigui

Original paper published in : Energy Conversion and Management 76 (2013) 437–452
https://doi.org/10.1016/j.enconman.2013.07.065

Optimal Energy Management of HEVs with Hybrid Storage System

E. Vinot, R. Trigui .
French institute of sciences and technology for transport, development and networks (IFSTTAR).
25 Avenue F. Mitterrand. 69675 Bron, France.
Corresponding author: emmanuel.vinot@ifsttar.fr

Abstract

Energy storage systems are a key point in the design and development of electric and hybrid vehicles. In order to reduce the battery size and its current stress, a hybrid storage system, where a battery is coupled with an electrical double-layer capacitor (EDLC) is considered in this paper. The energy management of such a configuration is not obvious and the optimal operation concerning the energy consumption and battery RMS current has to be identified. Most of the past work on the optimal energy management of HEVs only considered one additional power source. In this paper, the control of a hybrid vehicle with a hybrid storage system (HSS), where two additional power sources are used, is presented. Applying the Pontryagin's minimum principle, an optimal energy management strategy is found and compared to a rule-based parameterized control strategy. Simulation results are shown and discussed.

Applied on a small compact car, optimal and ruled-based methods show that gains of fuel consumption and/or a battery RMS current higher than 15% may be obtained. The paper also proves that a well tuned rule-based algorithm presents rather good performances when compared to the optimal strategy and remains relevant for different driving cycles. This rule-based algorithm may easily be implemented in a vehicle prototype or in an HIL test bench.

Keywords: Hybrid Electric Vehicle, hybrid storage systems, battery and electrical double-layer capacitor coupling, energy management

1. Introduction

Environmental issues are pushing the transportation sector to improve the efficiency of road-vehicles. Hybrid Electric Vehicles (HEVs) have a high potential to reduce fuel consumption and emissions. Due to their ability to recover kinetic energy while braking and to operate the engine in a more efficient area, CO_2 emissions can be reduced [1-3].

The energy management and component sizing are critical factors to achieve a high energetic performance (fuel consumption). The cost and lifetime of batteries is a negative aspect, which prevents HEVs from being competitive in the market.

To reduce the battery size and to avoid high battery current stress, a Hybrid Storage System – association of an electrical double-layer capacitors (EDLC,[4-6]) and batteries - can be used. In such a configuration, the battery can be designed to supply the energy while the EDLC is used for high power operations ([7-10]).

It is well known that EDLC associated with lead-acid batteries increase the regenerative braking capability of the storage system ([7]-11]), thus, the fuel economy could be increased. At the same time it is well documented that associating EDLC [with lead-acid battery can increase the battery lifetime. Depending on the application, a gain higher than 30% may be observed ([12-15]). Due to an extended lifetime and a better fuel economy, a storage system associating lead-acid battery and EDLC can be a viable economic alternative to Li-ion or NiMh batteries ([12-14]). The case of Li-ion associated with EDLC seems less convenient. The regenerative braking capability can be increased and it can provide benefits in terms of lifetime [5]. Nevertheless, the economic aspect of such an association seems currently not viable ([16], [17]) even if the reduction of the EDLC costs may change this statement [5].

The method proposed in this paper can be applied to different battery technologies, but the proposed example concerns only lead-acid and EDLC association (Section 4).

Off-line energy management optimization for HEVs with one electric energy source (a battery or EDLC) has been a major field of research in the last ten years and two well-known methods are commonly used: Dynamic Programming [18] and Pontryagin's minimum principle [19]. Although these methods can only be used in off-line simulation (drive cycle known in advance), they have two main advantages:

i) evaluation of the maximum potential fuel economy of hybrid power-trains

ii) enabling studies on optimal component sizing for the considered hybrid architectures[20]

Methods that are implementable in real time have also been developed, and some of them are based on results from these two off-line optimization methods. The results achieved with these methods are always sub-optimal.

Standard HEVs with two power sources have one degree of freedom to provide the required power output to the wheels. For HEVs with a Hybrid Storage System (HSS), an additional degree of freedom is introduced by adding a third power source. The energy management is therefore more complex and the optimal instantaneous power split between the three sources (fuel tank, battery, EDLC) is more difficult to be found. Some rule-based methods suggest the use of the EDLC for high power and/or high frequency output ([7-10,21-23]), while the battery power is limited and kept at low frequency as long as possible. However, to our knowledge, no previous research has studied the maximum potential of this hybrid architecture under optimal energy management.

The first idea to solve the optimisation problem is to try an extension of the well-known methods previously developed for the conventional HEV case. For dynamic programming, this means adding a second dimension to the battery State of Charge (SOC) graph that represents the EDLC Open Circuit Voltage (OCV) graph. This is numerically difficult because the computational cost grows exponentially with the number of dimensions. The Pontryagin's minimum principle theory, on the contrary, is more flexible because of its low computational effort. In addition, the optimization problem can easily be formulated.

In the following we will use this last approach that will be explained in detail until its application to the case of an HEV with HSS. As a result, the optimal energy management is found considering two objective functions to be minimized. These are the fuel consumption and the use of battery represented by the Root Mean Square (RMS) of the battery current. The Pareto front depending on these two costs is computed. Users may then choose a point on this front depending on the weight applied to fuel consumption and battery RMS current. In order to compare this optimal approach with possible real time performance, a rule-based energy management strategy was developed. A parametric study was carried out to improve the results of this method. Finally, a comparison

between the optimal off-line solution and the best-found implementable rule-based management strategy is shown.

2. Offline Energy Management optimization of HEVs with HSS

2.1. Global optimization problem definition

Generally, an HEV architecture (Fig. 1) is composed of a fuel tank, one or more additional power sources and a drive-train, which consists of an ICE, electrical machines (EM), clutches, gears, etc. The goal of the optimization is to find the operation of the different power sources which minimizes a given criterion, often the fuel consumption.

If the optimization is performed for an entire driving schedule, assumed to be known in advance, it is called global. Considering a driving cycle, such an algorithm determines the optimal energy management strategy for a given vehicle configuration. As a result, the maximum potential gains with respect to the objective function are determined. On the other hand, if no or only partial knowledge of future driving conditions is available, online energy management laws or instantaneous optimization algorithms can be applied. However these can only lead to suboptimal solutions.

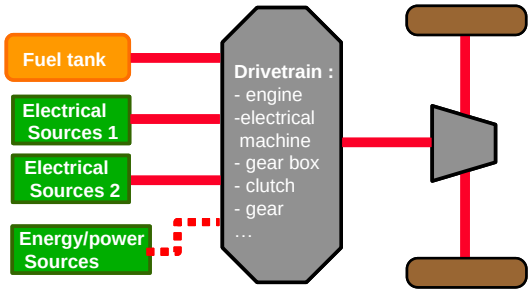

Fig. 1 : General architecture

In a global optimization approach, the variation of the stored energy between the beginning and the end of the driving cycle has to be taken into account for all additional power sources. In our case, for consumption evaluation, this variation is chosen to be equal to zero as the considered vehicle is a non Plug-in HEV that uses a charge sustaining strategy for the batteries.

Meanwhile, the developed algorithm can be extended to vehicles with other kinds of energy sources and could be applied to vehicles with energy depleting operation.

2.2. Optimization problem in backward approach

In this section we will define the optimization problem for the HEV case.

The aim of this optimization is generally to minimize the global fuel consumption of the HEV for a known driving cycle. Knowing that the fuel cost depends on the torque of the Internal Combustion Engine (ICE) and its rotational speed the cost criterion for a driving cycle can be represented by:

$$J = \min\left[\sum_{i=1}^{n} C_i(T_{ICE},\Omega_{ICE})\cdot T_s\right] \quad (1)$$

Where (T_{ICE}, Ω_{ICE}) are the ICE torque and speed, $C_i(T_{ICE}, \Omega_{ICE})$ is the fuel consumption for the time interval between $t = i*T_s$ and $t = (i + 1)*T_s$. T_s is the sampling time and n the number of samples in the cycle.

Knowing the driving cycle in advance, a backward approach (Fig. 2) can be used. Given the torque and speed of the wheel, calculating upstream through the drive-train, the operation of the engine and the electrical sources are calculated [20, 24-25].

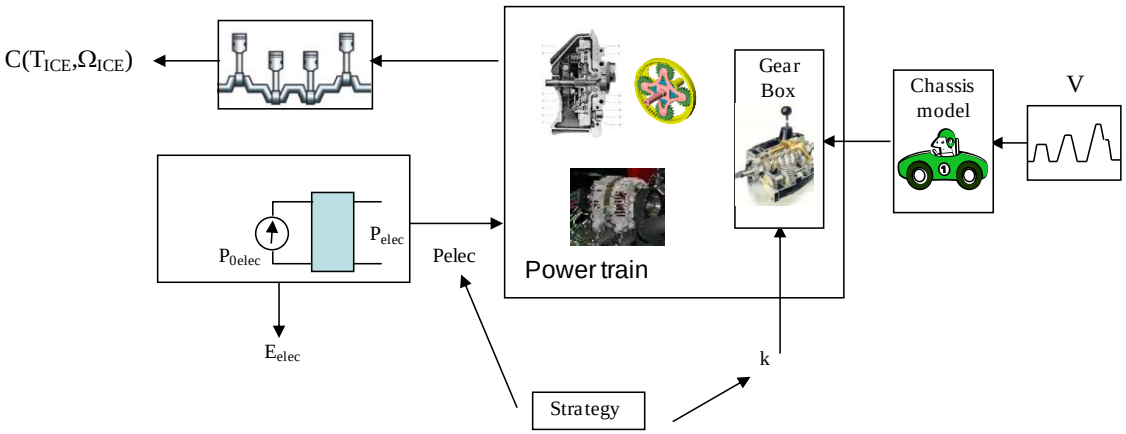

Fig. 2 : HEV backward principle

In such an approach, for each time step, we know the driving conditions which are defined by the wheel torque T_r and the wheel rotation speed Ω_r. To satisfy these driving requirements, the control unit has to make two decisions:

(1) The power split ratio between ICE, electrical sources and mechanical brakes (BR),

(2) The transmission ratio between the output shaft and the ICE, (in conventional vehicles this corresponds to the gear ratio).

In an optimal strategy, the mechanical brakes come into action only when the EM torque is at its maximum braking capacity, and cannot satisfy the required torque T_r to decelerate the vehicle.

In addition, power conservation laws and power-train constraints imply that:

- T_{ICE} (ICE torque), T_{BR} (Braking torque), T_{EM} (Electrical Machine torque), are linked to T_r (Required torque).
- Ω_{ICE} (ICE speed), Ω_w (wheel speed), Ω_{EM} (Electrical Machine speed) are linked by the gear ratio and other potential coupling relations ([25-26])
- T_{EM} is linked to the electrical power P_{elec} provided at the output of the electrical source.

In the following, a parallel HEV topology is considered and the gear will be imposed at each time step of the driving cycle. As for a given wheel condition (T_r, Ω_w) the ICE torque T_{ICE} depends only on P_{elec} (cf. section 4.2 Eq. (34) and Eq. (35)), and the ICE speed ω_{ICE} is fixed by the driving cycle and drive-train characteristics, the fuel cost consequently depends only on P_{elec}.

Therefore, the optimization problem may be expressed as follows:

$$J = \min\left[\sum_{i=1}^{n} C_i(P_{elec})\right] \quad (2)$$

with a constraint on the amount of electrical energy stored E_{elec} : $E_{elec\_end} - E_{elec\_ini} = \Delta E_{elec}$

It should be noted that for series architectures and power split architectures, like the Toyota Hybrid System, the gearbox ratio may be replaced by the speed of the electric generator, which is then treated as a local variable of optimization [20].

This optimization problem can be solved in two ways. The first method is the dynamic programming, which is based on the Hamilton-Bellman-Jacobi's (HBJ) functional equation, or more generally Bellman's principle of optimality [18-20]. The second method is based on Pontryagin's minimum principle [27-30].
In previous works, these methods have already been applied to HEV. For example, dynamic programming has been used to compute optimal energy management strategies for different hybrid power-train architectures with batteries in offline simulation [18,31]. Pontryagin's minimum principle has mainly been implemented for real-time management of parallel hybrid architectures [19, 32, 33] and fuel cell vehicle with battery or electrical double-layer capacitor [34]. In these cases, only sub-optimal results can be achieved. In the scope of this paper the application of this principle with two control variables is not investigated as Lagrange multipliers (key variables to be set in the Pontryagin's minimum method) are difficult to predict. This paper focuses on rule-based management easily implementable in real time while estimating their efficiency compared to the optimal energy management computed off-line using the Pontryagin's minimum method.

This paper highlights three specific points of application of the Pontryagin's principle:

- the consideration of a hybrid vehicle with two electrical sources: electrical double-layer capacitor and battery.
- the resolution of the problem by modeling the components using look-up tables rather than analytical models.
- the determination of Pareto optimal front between two objectives: fuel consumption and battery RMS current.

2.3. Problem solving using Pontryagin's minimum principle

In this part the Pontryagin's minimum principle is applied. First the main principles of this method are presented and then applied to the HEV with a hybrid storage system. Specifically the utilized battery and EDLC models are described.

2.3.1. General Principle

Let us consider a system defined by the following state equation:

Original paper published in : Energy Conversion and Management 76 (2013) 437–452
https://doi.org/10.1016/j.enconman.2013.07.065

$$\dot{x}(t) = \frac{dx(t)}{dt} = a(x(t), u(t), t) \tag{3}$$

and the functional J to be minimized:

$$J(u) = \int_{t_0}^{t_f} g(x(t), u(t), t)dt \tag{4}$$

where x (t) is the vector of state variables and u (t) the vector of control variables.

Imposing constraints on final time and final state (as in our case) the Pontryagin's minimum [27] principle can be used in the following way:

Given the augmented functional H, also called Hamiltonian:

$$H(x(t), u(t), p(t), t) = g(x(t), u(t), t) + p^T(t) \cdot a(x(t), u(t), t) \tag{5}$$

the necessary conditions for u* to be the optimal control are:

$$\begin{aligned} &(i) \quad \dot{x}(t) = \frac{\partial H(x(t), u^*(t), p(t), t)}{\partial p} \\ &(ii) \quad \dot{p}(t) = -\frac{\partial H(x(t), u^*(t), p(t), t)}{\partial x} \\ &(iii) \quad at\ each\ step\ of\ time\ and\ for\ all\ admissible\ control\ u(t) \\ &\quad H(x(t), u^*(t), p(t), t) \le H(x(t), u(t), p(t), t) \end{aligned} \tag{6}$$

Here p(t) is usually referred to the Lagrange multiplier and has to be determined in order to respect the constraints on the systems (cf part 3). $p^T(t)$ is the transpose of p(t).

The following points should be noted concerning these conditions:

- The first condition (i) represents the system equation (Eq.3)
- Together with the constraints of the system, the second condition (ii) allows the determination of the Lagrange multipliers (cf section 3.2)
- The third condition (iii) may be expressed as $\frac{\partial H(x(t), u(t), p(t), t)}{\partial u} = 0$, if the partial derivative with respect to u exists. Various works, where models with look-up tables were used, have implemented map fitting to find derivable functions in order to use this criterion ([19-32]). However, this is not necessary; the original condition (iii) with its inequality can be used by finding the minimum of the functional H with an iterative process for example.
- If the second partial derivative of H with respect to u exists, then the condition $\frac{\partial^2 H(x(t), u(t), p(t), t)}{\partial u} > 0$ is sufficient to guarantee that u* causes a local minimum of H.

A key point of this method is if p(t) is known, the global minimization problem is reduced to a minimization of a local functional H. The determination of p(t) will be performed iteratively to respect the constraints (cf. section 3.2).

Original paper published in : Energy Conversion and Management 76 (2013) 437–452
https://doi.org/10.1016/j.enconman.2013.07.065

2.3.2. Hybrid electric vehicle with Hybrid storage system

The derived method will now be applied to a hybrid drive-train where an electrical double-layer capacitor is coupled with a battery (Fig. 3).

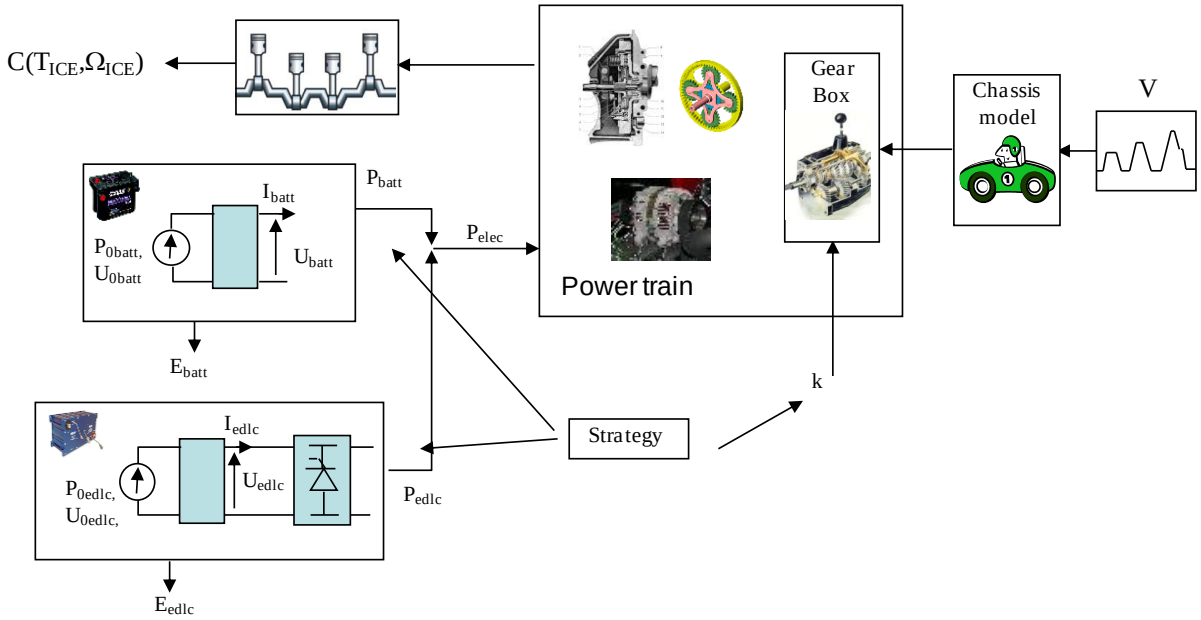

Fig. 3 : Battery and UC coupling

In this configuration at least one inverter is highly recommended to couple the two electrical sources. It seems that a bidirectional DC/DC converter placed on the EDLC side is a good solution ([5]), in terms of cost and efficiency. As the efficiency of such a device is relatively high and quite constant the corresponding losses are represented here by a constant efficiency.

2.3.2.1. General electrical sources model

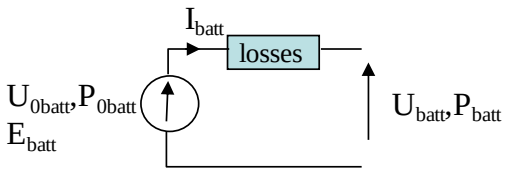

Fig 4 : Electrical source model

Fig. 4 shows the model of the electrical sources used in this paper (in the case of a battery). It is composed of an electrical voltage source and a series impedance (section 2.3.3.1 and 2.3.3.2) to take into account ohmic losses, faradic efficiency and possibly more complex phenomena (battery relaxation period …):

U_{0batt}: Open circuit voltage

E_{batt}, P_{0batt}: Stored energy and power of the perfect electrical source

U_{batt}, P_{batt}: Voltage and power at the output of the electrical source

In the case of a battery, the SOC (in %) is commonly defined as [37]:

$$SOC = \frac{-100}{3600 * C_{batt}} \int \eta_f I_{batt} dt \quad with\ \eta_f = 1\ if\ I_{bat} > 0 \tag{7}$$

Where I_{batt} is the battery current, η_f is the faradic efficiency, and C_{batt} the battery capacity in Ah.

In this paper, we also use the amount of stored energy E_{batt}:

$$E_{batt} = \int -\eta_f U_{0batt} I_{batt} dt \tag{8}$$

It should be noted that with Eq.7 and Eq.8 a SOC constraint can be defined using the energy constraint:

$$\Delta SOC = f(\Delta E_{batt}) \tag{9}$$

Thus, in the following, the SOC constraint is satisfied while solving the problem using the amount of stored energy E_{batt}.

In the same way, a constraint on the EDLC open circuit voltage can easily be defined using the EDLC amount of stored energy E_{EDLC} as :

$$E_{edlc} = \frac{1}{2} C U_{0edlc}^2 \tag{11}$$

2.3.2.2. Pontryagin's minimum principle application in HEV with HSS

Considering the case of an HEV (Fig. 3), the control variables u(t) are represented by the electric power vector P_{elec} which components are P_{batt} and P_{EDLC}. E_{batt} and E_{EDLC} make up the state variable vector x(t), from here on denoted E_{elec}. All the parameters used in the following equation are defined in the nomenclature table in the appendix.

The system's state equations may be expressed as:

$$\dot{E}_{elec}(t) = P_{0elec}(E_{elec}(t), P_{elec}(t), t)$$

$$with\ E_{elec} = [E_{batt} \quad E_{edlc}]$$
$$P_{0elec} = [P_{0batt} \quad P_{0edlc}]$$
$$P_{elec} = [P_{batt} \quad P_{edlc}] \tag{11}$$

$$\Rightarrow \begin{cases} \dot{E}_{batt} = P_{0batt}(E_{batt}(t), P_{batt}(t), t) = -\eta_f(E_{batt}) \cdot I_{batt}(t) \cdot U_{0batt}(E_{elec}) \\ \dot{E}_{edlc} = P_{0edlc}(P_{edlc}(t), E_{edlc}(t), t) = -I_{edlc}(t) \cdot U_{0edlc}(t) \end{cases}$$

$$E_{elec}(t) = \int_0^t P_{0elec}(t) dt = \int_0^t -\eta_f(E_{elec}) \cdot I_{elec}(t) \cdot U_0(E_{elec}) dt$$
$$with\ I_{elec} = [I_{batt} \quad I_{edlc}]$$
$$U_0 = [U_{0batt} \quad U_{0edlc}]$$
$$\eta_f = [\eta_{f\,batt} \quad 1] \tag{12}$$

The cost function to be minimized could be simple, such as fuel consumption, or could consist in a complex sum, for example fuel consumption plus emission plus battery RMS current. To minimize the global fuel

consumption, taking into account the battery RMS current a weighting method is used. The objective to be minimized is:

$$J = \int_0^T (C(P_{batt}, P_{edlc}) + K_{ibatt} \cdot I_{batt}^2(E_{batt}, P_{batt}))dt \tag{13}$$

Where $C(P_{batt},P_{edlc})$ is the fuel consumption which depends only on the electrical power composed of battery and EDLC power.

Minimizing the battery RMS current is equivalent to a minimization of the integrated square of the battery current along the cycle (Eq. (13)). Moreover the weighted objective can be proven to be Pareto optimal ([38,39]). In the case $K_{ibatt}=0$, fuel consumption alone is minimized. On the other hand, if K_{ibatt} is high enough, only the battery current is minimized and the battery is often not used at all.

In our case the Hamiltonian is defined by:

$$\begin{aligned} &H(E_{elec}, P_{elec}, k) = C(P_{batt}, P_{edlc}) + K_{ibatt} \cdot I_{batt}^2(E_{batt}, P_{batt}) + p(t) \cdot \dot{E}_{elec} \\ &H(E_{batt}, E_{edlc}, P_{batt}, P_{edlc}) = \\ &\quad C(P_{batt}, P_{edlc}) + Ki_{batt}^2(E_{batt}, P_{batt}) + p_1(t) \cdot P_{0batt}(E_{batt}, P_{batt}) + p_2(t) \cdot P_{0edlc}(E_{edlc}, P_{edlc}) \end{aligned} \tag{14}$$

$$\text{with } p(t) = [p_1(t) \quad p_2(t)]$$

The conditions of the Pontryagin's minimum principle are represented by:

$$(ii) \quad \dot{p}(t) = -\frac{\partial H(E_{elec}, P_{elec})}{\partial E_{elec}}$$

$$\Rightarrow \begin{cases} \dot{p}_1(t) = p_1(t) \dfrac{\partial P_{0batt}(E_{batt}, P_{batt})}{\partial E_{batt}} + K_{ibatt} \dfrac{\partial I_{batt}^2(E_{batt}, P_{batt})}{\partial E_{batt}} \\ \dot{p}_2(t) = p_2(t) \dfrac{\partial P_{0edlc}(E_{edlc}, P_{edlc})}{\partial E_{edlc}} \end{cases} \tag{15}$$

$$(iii) \quad \textit{at each step of time and for all admissible controls} [P_{batt}(t) \quad P_{edlc}(t)]$$
$$H(E_{batt}, E_{edlc}, P_{batt}^*, P_{edlc}^*) \leq H(E_{batt}, E_{edlc}, P_{batt}, P_{edlc})$$

Depending on the battery and EDLC models, the partial derivatives are then constructed and iteratively determined as presented in part 2.3.3.

In discrete time (8.ii) becomes:

$$\dot{p}(i) \equiv \frac{p(i) - p(i-1)}{T_s} \tag{16}$$

This leads to:

$$p_1(i) = \frac{p_1(i-1) + K_{ibatt}\frac{\partial I_{batt}^2(E_{batt},P_{batt})}{\partial E_{batt}}T_s}{(1+\frac{\partial P_{0batt}(E_{batt},P_{batt})}{\partial E_{batt}}T_s \quad)}$$
$$p_2(i) = \frac{p_2(i-1)}{(1+\frac{\partial P_{0edlc}(E_{edlc},P_{edlc})}{\partial E_{edlc}}T_s \quad)} \qquad (17)$$

Then ($p_1(0)$ and $p_2(0)$) have to be fixed in order to respect the constraints on the EDLC open circuit voltage and the battery SOC, (cf section 3.2). The expression of partial derivative terms $\partial I_{batt}^2/\partial E_{batt}$, $\partial P_{0batt}/\partial E_{batt}$ and $\partial P_{0edlc}/\partial E_{edlc}$ used in equation (15) and (17) depends on the model used for the battery and EDLC and are presented in the following section.

2.3.3. Battery and electrical double-layer capacitor model

In this section the partial derivative terms for ideal battery power, battery current squared and the ideal power of the EDLC in equation (15) are derived using the following battery and EDLC models.

2.3.3.1. Battery model

The battery model (Fig. 5) consists of an equivalent electric circuit with an open circuit voltage U_{0batt}, an internal serial resistance R_{batt}, and a faradic efficiency η_f. U_{0batt}, η_f and R_{batt} depend on the SOC (and thus the energy stored in the battery) and on the current using an experimental look up table.

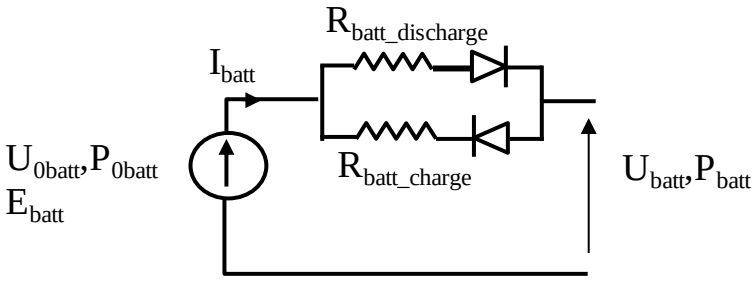

Fig. 4 : model of battery

The temperature is fixed for all the driving cycle but is chosen at the beginning of the cycle. In fact different look-up tables depending on the SOC and current can be used for different temperature. Nevertheless, no thermal model is used, and the parameters remain constant vs. temperature during all the driving cycle. This assumption seems acceptable as long as the driving cycle is short enough compared to the temperature rising time. In the same way, ageing can be taken into account if the battery has been characterized at different states of age [40].

It is noted that the dependence of U_{0batt} η_f and R_{batt} on SOC, battery current, temperature and life cycle are not included in the equation to avoid too complicated expressions.

As an example, a Lead Acid (Orbital from Exide) 40 Ah battery is presented as it is the battery used in the case study (part IV). The OCV is measured after 25 min rest, and the resistance is determined using temporal method of identification, i.e. the voltage drop during current pulse at different SOC. Figure 6 shows the measurement of the OCV and the charge/discharge resistance at 25°C. Figure 7 shows the OCV partial derivative of OCV along

the stored energy. The data are presented as a function of the energy stored in the battery, since this is the state variable of our problem.

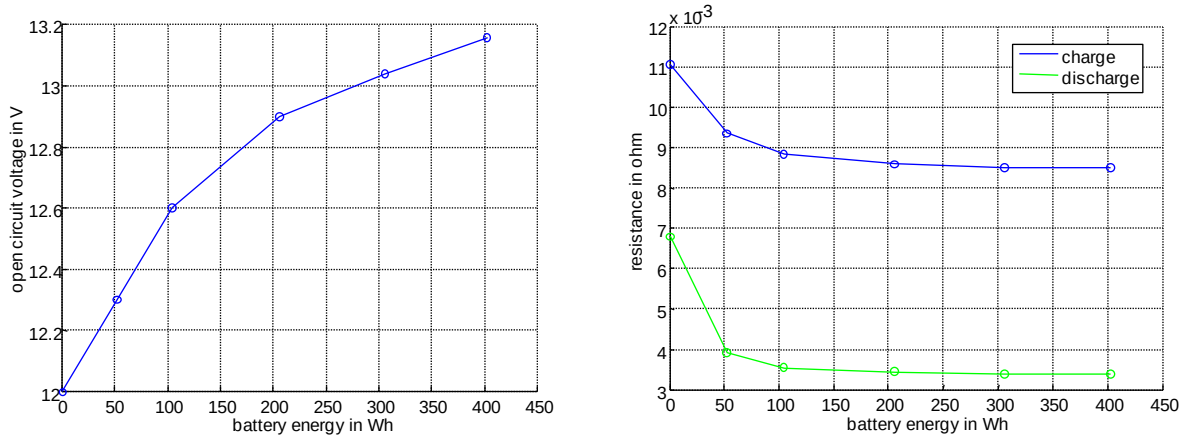

Fig. 5 : Open circuit voltage (left) and resistance (right) of a prismatic NiMh battery element.

It is clear that other battery types such as Li-ion or Ni-Mh for example can be used. The method remains perfectly valid without any change if the battery model is the same. This method can also be adapted for other more accurate models ([5 ,41-43]). In this case, the derivative of the battery power ideal sources and battery current squared along E_{batt} has to be calculated.

Using the model presented Fig. 5 and Ohm's law the battery power can be represented by:

$$\begin{aligned} P_{batt} &= U_{0batt} \cdot I_{batt} \\ P_{batt} &= (U_{0batt} - R_{batt} \cdot I_{batt}) I_{batt} \\ with &\begin{cases} R_{batt} = R_{batt\_charge} \ \ if \ \ I_{batt} < 0 \\ R_{batt} = R_{batt\_discharge} \ \ if \ \ I_{batt} > 0 \end{cases} \end{aligned} \tag{18}$$

And therefore:

$$I_{batt} = \frac{1}{2R_{batt}}(U_{0batt} - \sqrt{U_{0batt}^2 - 4P_{batt}R_{batt}}) \tag{19}$$

In addition

$$P_{0batt} = -\eta_f (P_{batt} + R_{batt} I_{batt}^2) = -\eta_f U_{0batt} \cdot I_{batt} \tag{20}$$

Using Eq. (19) and Eq. (20) the battery power of the ideal sources P_{0batt} can be computed by:

$$P_{0batt} = -\frac{\eta_f}{2R_{batt}}(U_{0batt}^2 - U_{0batt}\sqrt{U_{0batt}{}^2 - 4P_{batt}R_{batt}}) \tag{21}$$

The partial derivative of P_{0batt} and I^2_{batt} with respect to E_{batt} can then be expressed as a function of $\partial U_{0batt}/\partial E_{batt}$ (Fig. 7), $\partial \eta_f / \partial E_{batt}$ and $\partial R_{batt}/\partial E_{batt}$.

Original paper published in : Energy Conversion and Management 76 (2013) 437–452
https://doi.org/10.1016/j.enconman.2013.07.065

$$\frac{\partial P_{0batt}}{\partial E_{batt}} = -\frac{\eta_f}{2R_{batt}}\left[2U_{0batt}\frac{\partial U_{0batt}}{\partial E_{batt}} - \frac{\partial U_{0batt}}{\partial E_{batt}}\sqrt{U_{batt0}{}^2 - 4P_{batt}R_{batt}} - \frac{U_{0batt}^2\frac{\partial U_{0batt}}{\partial E_{batt}}}{\sqrt{U_{0batt}{}^2 - 4P_{batt}R_{batt}}}\right]$$
$$+\frac{1}{2R_{batt}}\left(\frac{\eta_f}{R_{batt}}\frac{\partial R_{batt}}{\partial E_{batt}} - \frac{\partial \eta_f}{\partial E_{batt}}\right)\left[U_{0batt}^2 - U_{0batt}\sqrt{U_{0batt}{}^2 - 4P_{batt}R_{batt}}\right] - \frac{\eta_f}{2R_{batt}}U_{0batt}\frac{4P_{batt}\frac{\partial R_{batt}}{\partial E_{batt}}}{2\sqrt{U_{0batt}{}^2 - 4P_{batt}R_{batt}}} \quad (22)$$
$$\frac{\partial I_{batt}^2}{\partial E_{batt}} = \frac{1}{2R_{batt}{}^2}\left(U_{0batt} - \sqrt{U_{0batt}^2 - 4P_{batt}R_{batt}}\right)\left[\frac{1}{R_{batt}}\frac{\partial R_{batt}}{\partial E_{batt}}\left(U_{0batt} - \sqrt{U_{0batt}^2 - 4P_{batt}R_{batt}}\right) + \frac{\partial U_{0batt}}{\partial E_{batt}} - \frac{U_{0batt}\frac{\partial U_{0batt}}{\partial E_{batt}}}{\sqrt{U_{0batt}{}^2 - 4P_{batt}R_{batt}}} + \frac{2P_{batt}\frac{\partial R_{batt}}{\partial E_{batt}}}{\sqrt{U_{0batt}{}^2 - 4P_{batt}R_{batt}}}\right]$$

U_{0batt}, η_f and R_{batt} are functions which vary with the SOC. Once $\partial\eta_f/\partial E_{batt}$, $\partial R_{batt}/\partial E_{batt}$ and $\partial U_{0batt}/\partial E_{batt}$ are determined this expression is easily implementable with existing software.

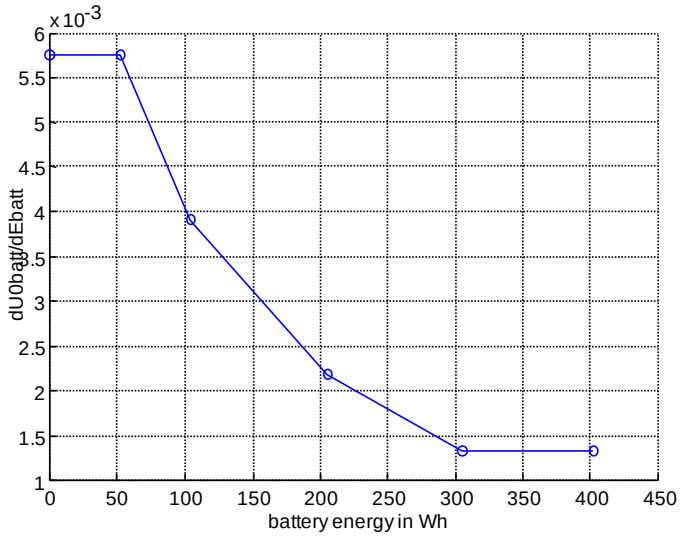

Fig. 6 : OCV partial derivative along stored energy

2.3.3.2. EDLC model

The EDLC model is presented in Fig. 8. A simple model composed of one main capacity in series with a parallel R_xC_x and main resistor R_{EDLC} is used ([44]). No self-discharge is considered as the time constant of this phenomenon is high compare to the time of the driving cycle used in this study. The parameters have been determined using temporal identification with pulse current method. R_{EDLC} is determined by the voltage drop. The R_xC_x represent exponential behavior with time constant around 0.1 s. These parameters are independent of the charge of the EDLC and of the current. A constant DC/DC efficiency η_{DCDC} is considered.

Original paper published in : Energy Conversion and Management 76 (2013) 437–452
https://doi.org/10.1016/j.enconman.2013.07.065

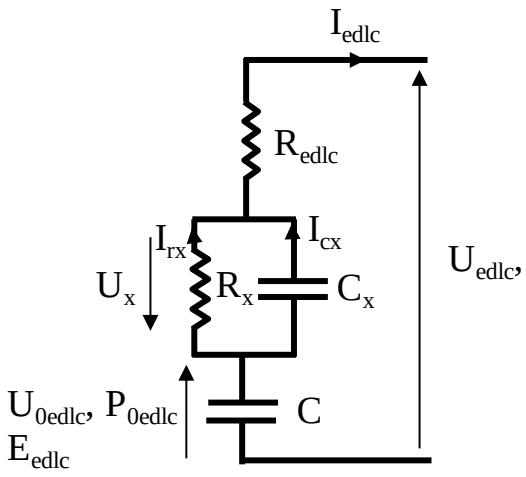

Fig. 7 : model of UC

As for the battery, more accurate models can be used as long as the derivative of the EDLC power ideal sources along E_{edlc} can be calculated. For example, the DC/DC converter efficiency may be function of E_{edlc}.
In order to use equation (11) P_{0EDLC} has to be expressed as a function of E_{EDLC} and P_{EDLC}.
Using the model Fig. 8 and the Kirchhoff and Ohms laws we calculate:

$$\begin{aligned} I_{cx} &= C_x \frac{dU_x}{dt} \\ I_{Rx} &= \frac{U_x}{R_x} \\ I_{edlc} &= I_{cx} + I_{Rx} \end{aligned} \tag{23}$$

For a given EDLC current I_{EDLC}, the current I_{CX} in the capacitor C_x is easily derived from Eq. (23):

$$\begin{aligned} I_{cx} &= -(\frac{U_{x0}}{R_x} - I_{edlc}) \cdot e^{-\frac{t}{\tau_x}} \\ with\ \tau_x &= R_x \cdot C_x \end{aligned} \tag{24}$$

Then the power in the main capacity C can be expressed as the sum of the power in each component:

$$P_{0uedl} = U_{0edlc} I_{edlc} = (P_{edlc} + R_{edlc} I_{edlc}^2 + \frac{U_x^2}{R_x} + U_x I_{cx}) \tag{25}$$

Thus using Eq.(24) and (25) the EDLC current is defined by:

$$I_{edlc} = -\frac{\sqrt{\frac{2E_{edlc}}{C}} - U_{x0} \cdot e^{-t/\tau_x} - \sqrt{(\sqrt{\frac{2E_{edlc}}{C}} - U_{x0} \cdot e^{-t/\tau_x})^2 - 4P_{edlc}(R_{edlc} + R_x(1 - e^{-t/\tau_x})}}{2(R_{edlc} + R_x(1 - e^{-t/\tau_x}))} \tag{26}$$

With the following definitions of R_e and U_0:

$$R_e = (R_{edlc} + R_x(1 - e^{-t/\tau_x})$$
$$U_0 = \sqrt{\frac{2E_{0edlc}}{C}} \quad (27)$$

$\frac{\partial P_{0edlc}}{\partial E_{edlc}}$ can be expressed as :

$$\frac{\partial P_{0edlc}}{\partial E_{edlc}} = -\frac{1}{R_e C}\left(1 - \frac{U_{x0}e^{-t/\tau_x}}{2U_{0edlc}} - \frac{U_{0edlc}^2 - 2U_{0edlc}U_{x0}e^{-t/\tau_x} - 2R_e\frac{P_{edlc}}{(\eta_{DC/DC})^{sign(Pelec)}} - \frac{1}{2}U_{x0}^2 e^{-2t/\tau_x}}{\sqrt{U_{0edlc}((U_{x0}e^{-t/\tau_x} - U_{0edlc})^2 - 4R_e\frac{P_{edlc}}{(\eta_{DC/DC})^{sign(Pelec)}})}}\right) \quad (28)$$

Where sign(Pelec) is the sign of the electrical power.

With the derived equations the optimization problem can be solved using Pontryagin's minimum principle.

3. Numerical Resolution of the problem

As presented in the previous section, applying Pontryagin's minimum principle, two actions to solve the problem have to be performed in combination:

- At each time step, the minimum of the Hamiltonian with respect to battery current and EDLC current has to be found.
- The initial values of the Lagrange multipliers have to be identified to take into account the constraints on battery SOC and EDLC open circuit voltage (section 2.3.1).

3.1. Minimum of Hamiltonian

To illustrate the described method, a parallel mild hybrid architecture with two clutches is used (Fig. 13). For the vehicle subsystems modeling, the components of the VEHLIB library [45] were used. Fuel consumption and machine losses are modeled by experimentally identified look-up tables. The NEDC cycle (New European Driving Cycle, Fig. 9) is a common reference in Europe and was chosen here for its simplicity in analyzing results.

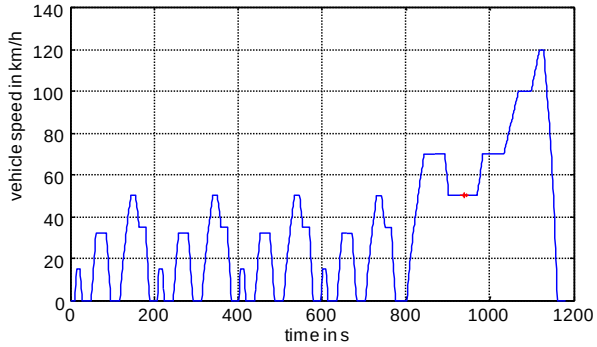

Fig. 8 : NEDC Cycle

For a given vehicle configuration (described in part 4), Fig. 10 shows the shape of the Hamiltonian at one instant of the NEDC cycle (here t=940s). As it can be seen, it is possible that the Hamiltonian, which is a function of

battery and EDLC current, contains several local minima. In order to find the global minimum a matrix approach was used; battery and EDLC current are sampled so that a grid is obtained on which the minimum is found (with a precision relative to the grid steps).

The pure electric mode is treated separately. In this case the global electrical power is imposed and the resulting Hamiltonian can be represented by a curve (red line Fig. 11). The two minima of the surface (hybrid mode) and the curve (pure electric mode) are identified and compared. The minimum of the two is chosen and with this the operating mode and the share of power between ICE, Battery and EDLC is specified.

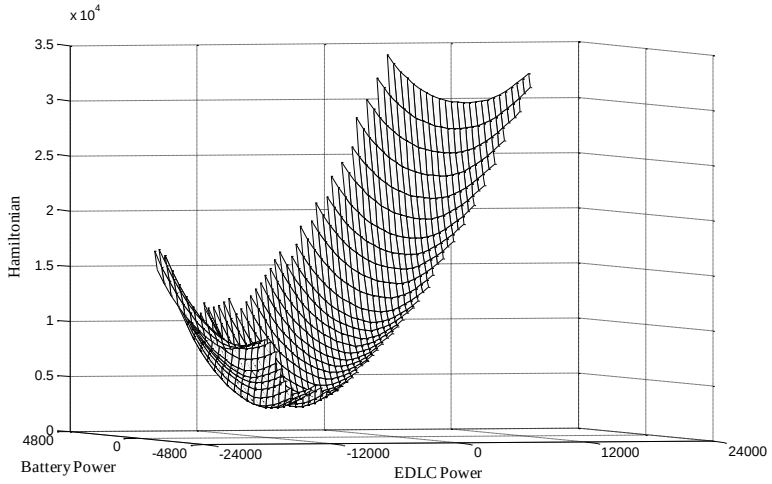

Fig. 9 : Hamiltonian in Hybrid mode at time 940.

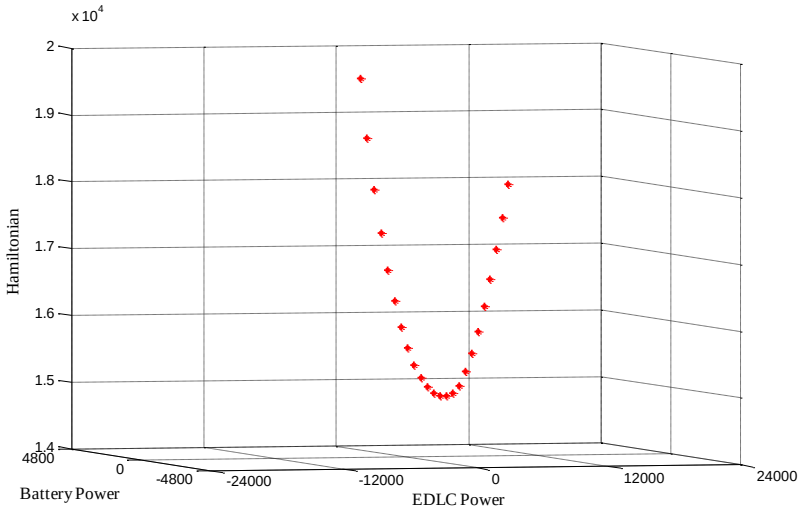

Fig. 10 : Hamiltonian in Electric mode at time 940.

3.2. Initial value determination for Lagrange multipliers

Using the Hamiltonian previously defined (Eq.14), two Lagrange multiplier values have to be identified in order to respect the two constraints on battery and EDLC OCV variation. One way to define the initial values p1(0) and p2(0) is to fix their ratio and then iteratively locate the p1(0) value such that the constraint on the battery

SOC variation is fulfilled. Repeating this process for different ratios allows us to choose the ratio which minimizes the EDLC OCV variation as well.

It should be noted that usually the battery energy is far greater than the EDLC energy. Therefore it is energetically more important to satisfy the constraint on the battery SOC than the constraint on the EDLC OCV. In Fig. 12 an example of this process is shown. Here p1(0) has been identified so that the SOC deviation on the whole cycle is zero. For varying ratios p2(0)/p1(0) the figure shows the EDLC and battery SOC variation ΔSOC (i.e. the soc difference between the initial and final SOC). EDLC SOC is defined as 100% corresponds to maximum EDLC OCV. In order to respect a zero SOC deviation of the EDLC, the choice of p2(0)/p1(0) in this case is about 0.97, which leads to p1(0)=3.180 and p2(0)=3.326.

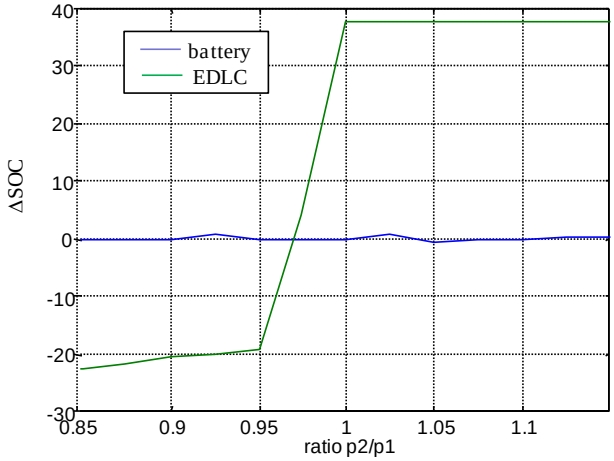

Fig. 11 : battery and EDLC SOC variation in %

4. Results and discussion

4.1. Case study

To illustrate the previous method, the case of a parallel mild hybrid architecture (Fig. 13) with two clutches is presented.

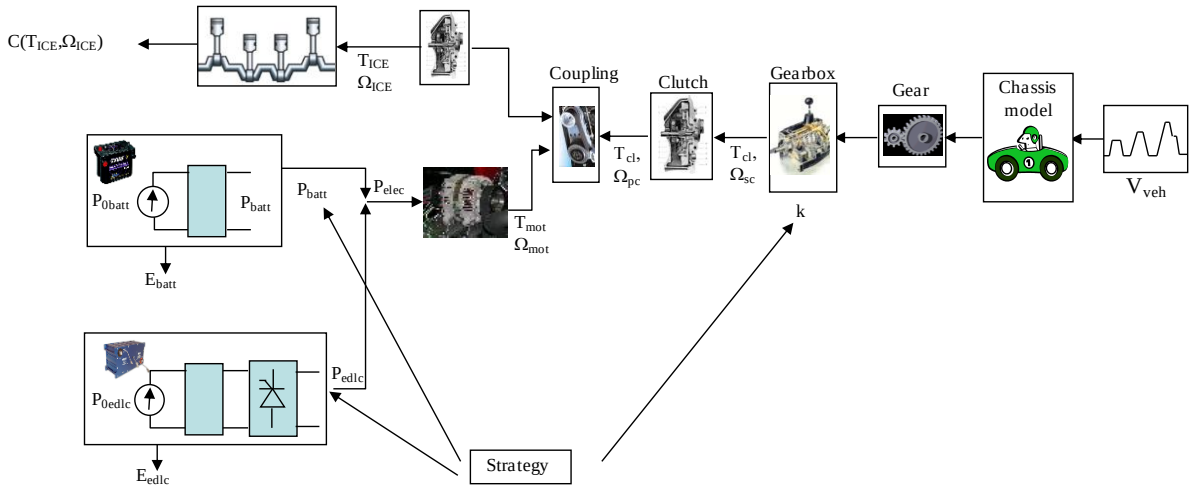

Fig. 12 : Parallel two clutches architecture.

The vehicle is a small compact car with the power-train characteristics presented Table 1.

This architecture was tested in our laboratory on HIL test bench ([46]) in the scope of a project in collaboration with Valeo ([47]). The components are those of a Renault Clio small compact car. This project tends to prove that a conventional architecture with only a boosted starter-alternator motor presents good performances in fuel economy. Only one battery block of 12V was used to simulate a conventional architecture with one lead-acid starter battery. Even if the components are now no longer available in our test bench we disposes of a validated simulation model of this architecture and its components.

In the scope of this paper, a pack of EDLCs, and a bidirectional buck DC/DC converter ([5,35,36]) are added to this architecture. In fact the resulting architecture remains a conventional vehicle with slight modifications. Thus this system may be easily implemented on the base of an existing vehicle.

A pack of 18 EDLCs was used because this is an available size for off-the-shelf EDLCs components from Maxwell.

Obviously the proposed method can be applied to other component sizes or vehicle configurations.

Table 1

Vehicle parameters

Vehicle weigh	1073kg
ICE power	54 kW @ 4000 rpm
EM power	15 kW @ 4000 rpm
ratio (EM speed/ICE speed)	2
Battery type	Lead Acide (Orbital from exide) 40Ah
Battery max/min current	300/-105 A
EDLC type	Maxwell 144 F
Ultracapacitor max/min voltage	48/22 V
Ultracapacitor max/min current	500/-500 A

4.2. Backward model of a parallel HEV architecture

This section presents the model of the components used in the simulation and the linked equation to calculate in a backward way the electrical power required on the electrical network.

From the driving cycle (Fig. 9), the wheel speed (ω_w), is known at each instant. The wheel torque (T_w) is then calculated using the vehicle model:

$$T_w = J_{veh}\frac{d\omega_w}{dt} + T_f \tag{29}$$

Where T_w is the wheel torque, T_f is the load torque calculated from the resistant forces, and ω_w is the wheel speed. J_{veh} is the overall inertia of the vehicle brought back to the wheels :

$$J_{veh} = M_{veh}R_w^2 + 4J_w \tag{30}$$

Where M_{veh} is the global weight of the vehicle, R_w is the wheel radius and J_w the inertia of one wheel.
T_f is calculated using chassis model i.e. aerodynamic coefficient and rolling resistance of the tire:

$$T_f = R_w \cdot ((a + a_r)V^2 + b_r V + c_r) \tag{31}$$

Where R_w is the wheel radius, V the vehicle speed, a, the aerodynamic coefficient of the chassis, and a_r, b_r, c_r the rolling resistance coefficients.
The torque relation on the shaft of the clutch (T_{cl}) is:

$$T_{cl} = \frac{T_w}{\eta_{trans}^{sign(T_w \cdot \omega_w)} R_{trans} \eta_{gb}^{sign(T_w \cdot \omega_w)} R_{gb}} \tag{32}$$

Where η_{trans} is the efficiency of the transmission (axle plus gear) and R_{trans} is the transmission ratio. $Sign(T_w.\omega_w)$ is the sign of the wheel power. η_{gb} and R_{gb} are the efficiency and ratio of the gear box. One efficiency value and one ratio are affected to each gear number.
The clutch model assumes that the torque T_{cl} is completely transmitted when the clutch is locked and that there is no speed sliding between the primary and the secondary speed of the clutch (ω_{pc} and ω_{sc}). In our case study, there is no gear between ICE and clutch i.e. they are on the same shaft. Thus, if the ICE minimum speed is higher than the speed imposed on the clutch by the wheel speed and gear ratio there is sliding. Otherwise, there is no sliding and no losses in the components. ω_{ICE} is then defined by:

$$\omega_{ICE} = \omega_{pc} = \min(\omega_{ICE\ -\min}, \omega_{sc}) \tag{33}$$

The speed of the electrical motor ω_{mot} is calculated using the gear ratio of the coupling device. The torque T_{mot} is determined using the look up table of the machine losses depending on the control variable P_{elec} and the speed.

$$T_{mot} = \frac{P_{elec} - losses(P_{elec}, \omega_{mot})}{\omega_{mot}} \tag{34}$$

The ICE torque is:

$$T_{ICE} = T_{cl} - R_{coup} \eta_{coup}^{sign(T_{mot} \cdot \omega_{mot})} T_{mot} \tag{35}$$

Where, η_{coup} is the efficiency of the coupling device and R_{coup} is the ratio. $Sign(T_{mot}.\omega_{mot})$ is the sign of the electrical machine power.
The fuel consumption $C(P_{elec})$ is then deduced using a look up table ([25]).

4.3. Comparison between HSS solution and battery only solution

A study has been performed to compare the performance of the hybrid configuration with battery and EDLC to that of a hybrid vehicle that uses only a battery. This allows us to show the advantages of the HSS system. The comparison is carried out using the models described above and the Pontriagyn's minimum principle method applied to each configuration.
Fig. 14 shows the Pareto optimal front of the two storage configurations (fuel consumption vs. RMS battery current) for the NEDC cycle and a real-life urban driving cycle. The Pareto front is obtained by varying the weighting factor of battery RMS current (Eq. 13). Globally, better fuel consumption is obtained for similar battery current in the case of the HSS. For a given RMS battery current, a gain in fuel consumption between 15% and 25% can be noted in the case of HSS. Similarly, the RMS current can be reduced with a compromise of higher fuel consumption.

Original paper published in : Energy Conversion and Management 76 (2013) 437–452
https://doi.org/10.1016/j.enconman.2013.07.065

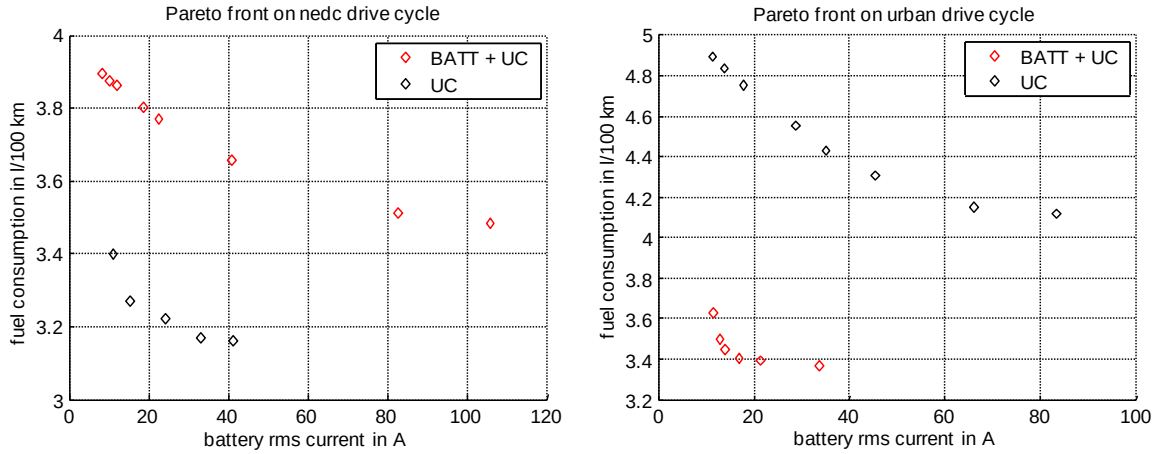

Fig. 13: Pareto front in NEDC and urban driving cycle with and without EDLC.

It has been shown in previous studies that HSS can increase the lifetime of lead-acid batteries by 30% and more ([12-14]). However, this depends strongly on the technology and on the battery usage. It is therefore difficult to predict the lifetime gain accurately. Considering the potential gains in fuel economy and lifetime, solutions such as HSS systems that combine lead-acid batteries with EDLC are worth studying as an alternative to Li-ion solutions ([12-14]).

The rest of the paper deals with a good and simple way to implement an energy management law of the overall system in the vehicle that can give fuel economy results close to the expected optimal one.

4.4. Comparison with parameterized rule-based method

The previously presented optimization method can be applied only off-line because the computation effort is too high to be implemented on-line. To implement a real time method, we propose here a rule-based method. The parameters of this method are tuned to obtain an efficient control and the results are compared with the optimal method.

4.4.1. Presentation of the rule-based method

Fig. 15 presents the rule-based strategy principle. It consists in two main steps.

In the first step the operating mode (electric or hybrid) and the required electrical power P_{elec} are fixed. This part is comparable to a load-following charge-sustaining strategy as in the parallel hybrid vehicle case ([48]).

In the second step the power share between battery and EDLC, i.e the battery target power P_{batt}, is defined.

Various management strategies of hybrid storage systems have been proposed ([7-9, 21, 22]). In this paper, a low-pass first order filter approach is used [21, 35].

Original paper published in : Energy Conversion and Management 76 (2013) 437–452
https://doi.org/10.1016/j.enconman.2013.07.065

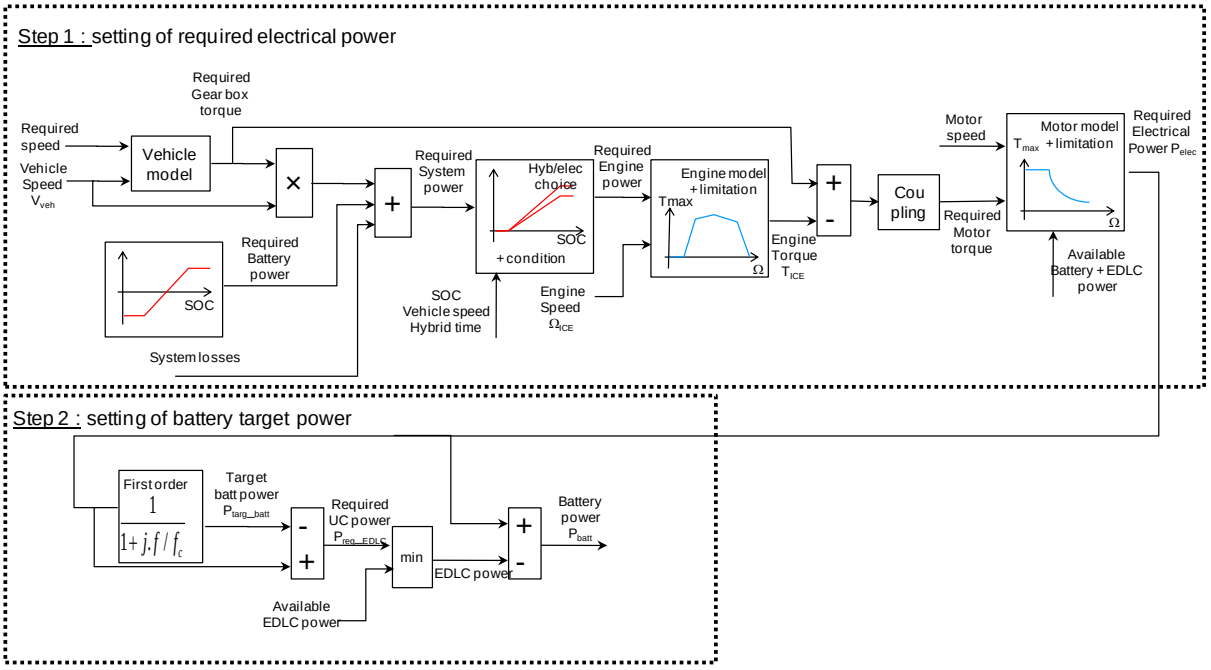

Fig. 14: Rule-based management strategy

To apply such a strategy in real time, a bidirectional DCDC converter placed between the battery and the EDLCs is used. Then the control management (developed below) provides a EDLC required current (or power) which is performed using a closed loop control on the DCDC converter duty cycle.

Step 1:

Given the current speed and the desired speed, the torque and power at the gear box is calculated using the developed vehicle model ([48]). Depending on the SOC of the battery, a desired battery power (negative or positive) P_{req_batt} is defined and added to the required vehicle power.

This vehicle is operated in hybrid (ICE on) or electrical mode (ICE off, where only battery and EDLC provide power). The choice between the two modes is made depending on two different parameters: the required power versus battery SOC curve and the vehicle speed. In general operation, a function of power versus battery SOC is given (ICE switch on power, Fig. 16a). If the total required vehicle power is lower than this curve for the current SOC the vehicle is operated in electrical mode. The hybrid mode is used if the required vehicle power exceeds this curve. However if the vehicle speed is higher than the maximal electrical vehicle speed, the vehicle is forced into hybrid mode. If the mode is changed from hybrid to electric mode, the time passed in hybrid mode first has to be validated. This constraint is imposed to reduce frequent changes between modes.

Knowing the required system power and operating mode (electrical/Hybrid), the engine torque is calculated (zero in electric mode), and the electrical motor torque can be evaluated. Thus, using motor losses and performances model, the required electrical power P_{elec} is known.

Step 2:

Once the required electrical power is fixed, the second step has to decide the power sharing between battery and EDLC. Here a first order low pass filter with a cut-off frequency f_c is used on P_{elec} to compute the battery target power P_{targ_batt}.Taking into account the available EDLC power, the EDLC is then used to provide the difference

between P_{targ_batt} and P_{elec}. If the desired EDLC power exceeds the available EDLC power (maximum/minimum current and/or voltage) the battery is used to provide the necessary additional power to fulfill P_{elec}.

Overall, with this strategy the battery satisfies the mean required power while high frequency power peaks are provided by the EDLC. Moreover, if P_{req_batt} is correctly tuned (part 4.4.2) the charge sustaining mode is guaranteed.

This behavior can be ensured using a specific battery power vs. SOC characteristic. As seen in Fig. 16 such a characteristic would discharge the battery (positive P_{req_batt}) when the SOC is high, and charge the battery (negative P_{req_batt}) if the SOC is low.

With this approach, at high SOC, the battery tends to discharge in boost mode (battery and engine provide power to the wheels). The boost mode is not necessarily a very efficient operation. We can inhibit this mode by setting the high threshold (P_{req_max}) to zero. At low SOC battery tends to be recharged using the engine.

Note, if the required power cannot be provided by the engine alone, the electric motor has to be operated in boost mode (within the scope of the system capability).

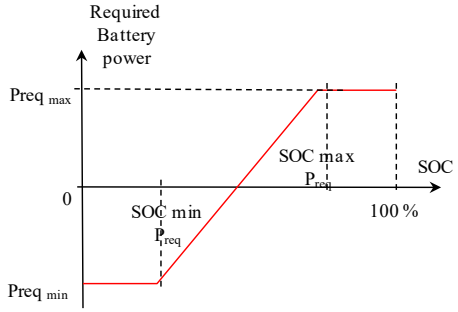

Fig. 16a

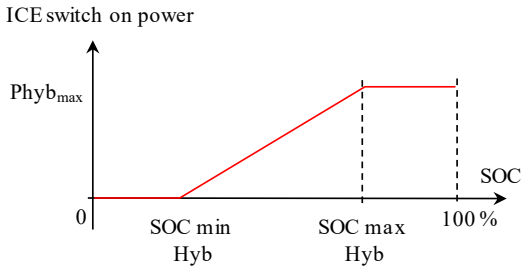

Fig. 16b

Fig. 15: Parameterized management curves

4.4.2. Parametric studies of the rule-based method

One problem using a rule-based approach is to find good values for the different control parameters in order to achieve an efficient control. Here the characteristics of the required battery power vs. SOC (Fig. 16a) and ICE switch on power vs. SOC (Fig. 16b) will be defined using seven parameters (Table 2

Table 2). The cut-off frequency of the low-pass filter is used as a parameter as well.

A parametric study has been performed on 8 parameters (Table 2

Original paper published in : Energy Conversion and Management 76 (2013) 437–452
https://doi.org/10.1016/j.enconman.2013.07.065

Table 2). A range and step size were chosen for each parameter. For each combination of these, an iterative method was used to find the initial battery SOC and EDLC open circuit voltage that lead to charge sustaining operation ($\Delta SOC<0.1$ % and $\Delta U_{0EDLC}<1$ V).

Table 2

Parameters and their values

Parameters	Symbols	Min value	Max value	step	units
Elec/hyb power High Threshold	$Phyb_{max}$	0	25000	2500	W
Elec/hyb soc low Threshold	$SOCmin_{Hyb}$	0	50	10	%
Elec/hyb soc High Threshold	$SOCmax_{Hyb}$	60	100	10	%
Battery required power High Thresholds	$Preq_{max}$	0	5200	1300	W
Battery required power low Thresholds	$Preq_{min}$	0	2500	1250	W
Battery required soc low Thresholds	$SOCmin_{Preq}$	0	50	10	%
Battery required soc High Thresholds	$SOCmax_{Preq}$	60	100	10	%
Low pass filter cutt off frequency	f_c	0.002	0.02	0.002	Hz

Fig. 17 and Fig. 18 show the fuel consumption versus RMS battery current for the resulting points, which respect the described constraints. The different colors in Fig. 17 represent groups with the same cut-off frequency. To simplify the figure, only selected values of cut-off frequency are presented. In Fig. 18, points with the same color represent results with equivalent required battery power ($Preq_{min}$) selected values.

Fig. 17 shows that the RMS battery current is highly influenced by the cut-off frequency as the clouds of points goes to smaller battery current when the cut-off frequency decreases. Note that under 0.0005 Hz the cut-off frequency seems to have no effect.

As seen in Fig. 18 the required battery power $Preq_{min}$ has a strong influence on fuel consumption. Values in the range of 2600 and 3900 W of required battery power seem to be significant for the minimization of the fuel consumption. Higher values are not considered because the maximum battery capability in the regeneration phase is 1300 W and therefore these values would saturate the required power.

The other parameters appear to have only minor influence (P_{reqmax}, $SOCmin_{preq}$, $SOCmax_{preq}$ $SOCmin_{hyb}$, $SOCmax_{hyb}$) or they affect the fuel consumption as well as the RMS current. For example the hybrid mode required power (P_{hybmax}) presents good compromises for all of its values (Fig. 19).

It is noted that for RMS current values higher than 60 A the fuel consumption increases. This may be explained by an increase in battery losses considering that in charge sustaining strategy the energy of the vehicle is finally

only provided by fuel. Moreover, in the optimal management (Fig. 14), the Pareto front starts at 40 Amps and points with higher RMS current and small fuel consumption do not exist (become not optimal).

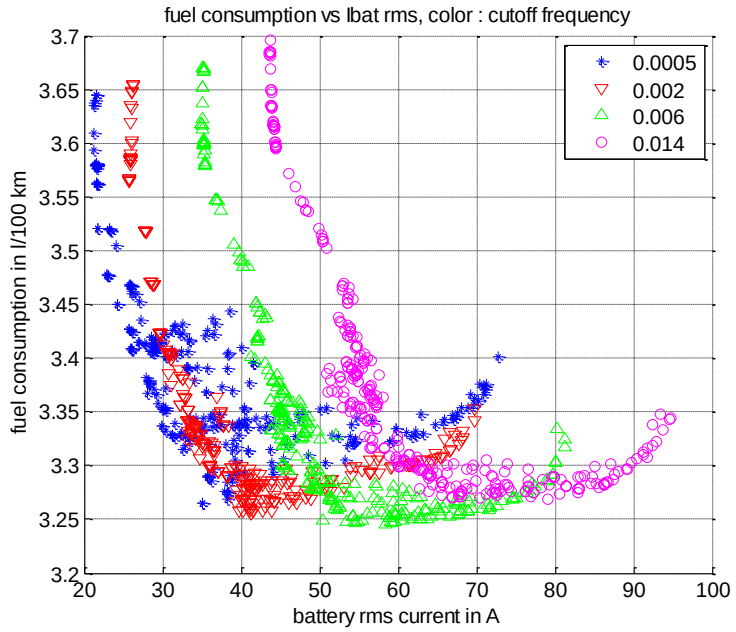

Fig. 16: Fuel Consumption vs Battery RMS current for different cut-off frequency.

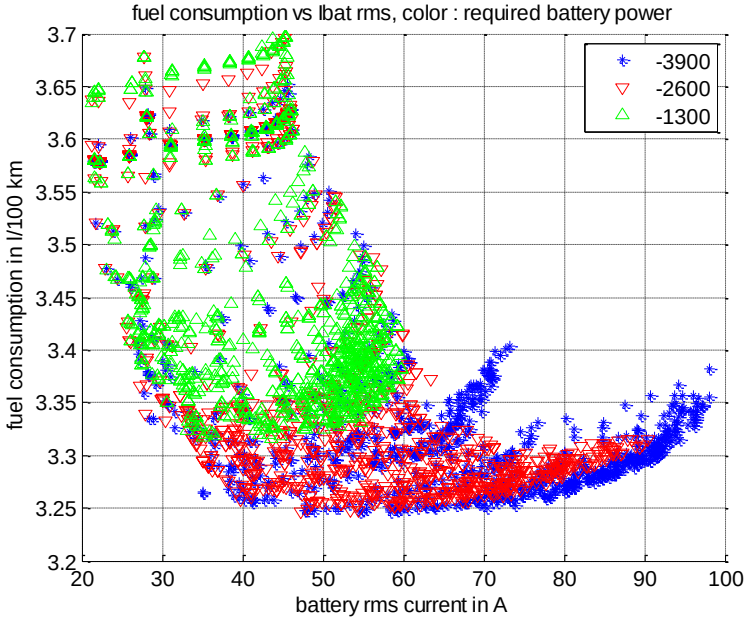

Fig. 17: Fuel Consumption vs Battery RMS current for different battery required power.

Original paper published in : Energy Conversion and Management 76 (2013) 437–452
https://doi.org/10.1016/j.enconman.2013.07.065

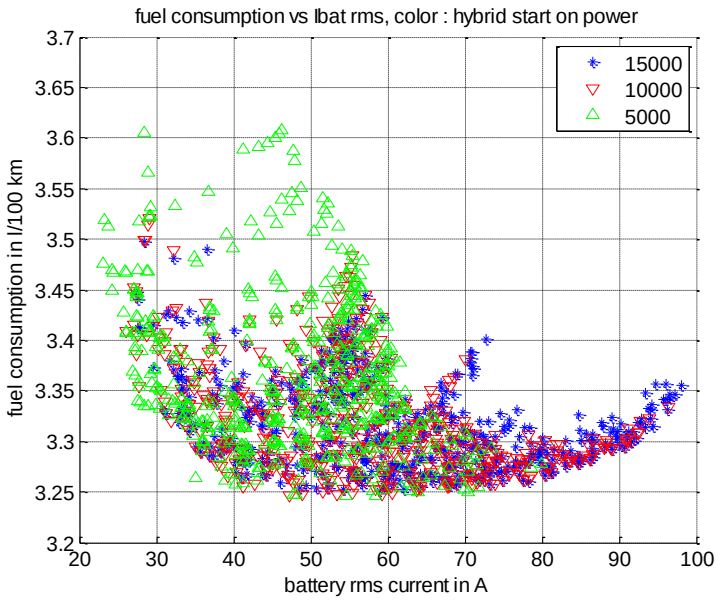

Fig. 18: Fuel Consumption vs Battery RMS current for different hybrid mode required power.

4.4.3. Comparison between optimal control theory and rule-based method

4.4.3.1. Fuel consumption and battery RMS current comparison on the NEDC cycle

As previously stated, the fuel consumption may not be the only objective to minimize. Using a weighted, two criteria objective function (Eq. (13)) allows to determine the Pareto optimal front optimized for fuel consumption and RMS battery current (cf. part 2.3.2.2).

Fig. 20 shows the fuel consumption versus battery RMS current for the result obtained by the rule-based parametric studies. The points marked in red where highlighted as they represent the most interesting tradeoff between fuel consumption and battery RMS current. The actual Pareto optimal front obtained using optimal control methods is shown here by the black diamond markers.

It becomes obvious for both cases that the point of minimum consumption is probably not the point of the most interest. A small compromise in fuel consumption allows for a drastic reduction in the battery RMS current. For the optimal control case, an increase in fuel consumption of 0.3 % decreases the battery RMS current by 19% (Table 3

Table 3). This tradeoff is even more important when using the rule-based method, where 0.5 % increases in fuel consumption allows to decrease battery RMS current by 40% (Table 4).

The rule-based method (even though improvable), shows good performances compared to optimal control. The fuel consumption is only 2-3% higher, which can be considered as a good performance, keeping in mind that a rule-based method is an online method where the cycle is not known in advance.

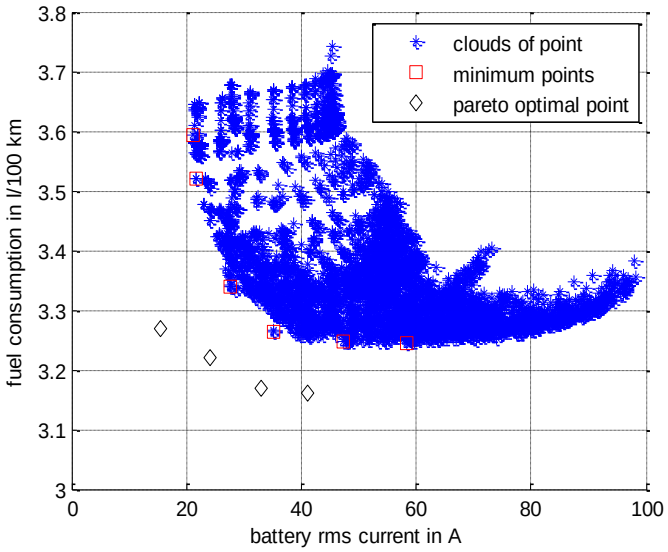

Fig. 19: Fuel Consumption vs Battery RMS current

Table 3

Points of the Pareto front

Optimal control				
K_{ibatt}	0	0.01	0.05	0.5
Fuel Consumption in l/100km	3.16	3.17(+0.3%)	3.22(+1.9%)	3.27(+3.5%)
Battery rms current in Amps	41.0	33.1(-19%)	24.0(-41%)	15.4(-62%)
K_{ibatt}: weighting factor of the objective function (cf part II.C.2)				

Table 4

Minimum points (red square) using rule-based method

Rule based control						
Fuel Consumption in l/100 km	3.245	3.246 (+0.03%)	3.26 (+0.5%)	3.34 (+2.9%)	3.52 (+8.5%)	3.59 (+10.5%)
Battery rms current in Amps	58.4	47.2 (-19%)	35.1 (-40%)	27.5 (-53%)	21.7 (-63%)	21.2 (-64%)
Cut-off frequency in Hz	0.06	0.04	0.0005	0.0001	0.0005	0.0005

4.4.3.2. Strategy and battery current stress comparison

To show the effect of the strategy on the battery current stress, this section presents comparisons of two rule-based strategies for two set of parameters (Fig. 21 and Fig. 22). Then a comparison of two strategies obtained using optimal control theory is presented (Fig. 23 and Fig. 24).

Fig. 21 and Fig. 22 show the differences in terms of strategies of power sharing and battery current stress for two sets of parameters of the rule based method (Table 2

Table 2):

- Strat 1 : set corresponding to the point of minimum of fuel consumption (first column of Table 4)
- Strat 2 : set corresponding to the point where a strong reduction of the RMS battery current was found when fuel consumption increased by a small amount (third column of Table 4)

Fig. 21 shows the development of the battery and EDLC current and battery SOC for the two strategies over the NEDC cycle.

In Fig. 22 the battery current stress i.e. the distribution of battery Ampere-hours (Ah) for the two strategies is shown. The amount of Ah given by the battery for different levels of battery current can be seen.

These figures highlight the effect of the cut-off frequency of the first order filter (Fig. 15, section 4.4.1) on the battery current. The battery current peak (Fig. 21) and the corresponding battery current stress (Fig. 22) are drastically reduced when the cut-off frequency is small (0.0005 vs 0.06 Hz). In the same time, the EDLC current does not change drastically. This explains a smoother SOC evolution associated to higher fuel consumption (8.5 %). However, analyzing the SOC (Fig. 21) the overall strategy does not changed so much. The electric mode is mostly used in the first 800 s of the cycle and for the rest of the cycle the engine is used to charge the battery to achieve charge sustaining operation over the cycle.

Original paper published in : Energy Conversion and Management 76 (2013) 437–452
https://doi.org/10.1016/j.enconman.2013.07.065

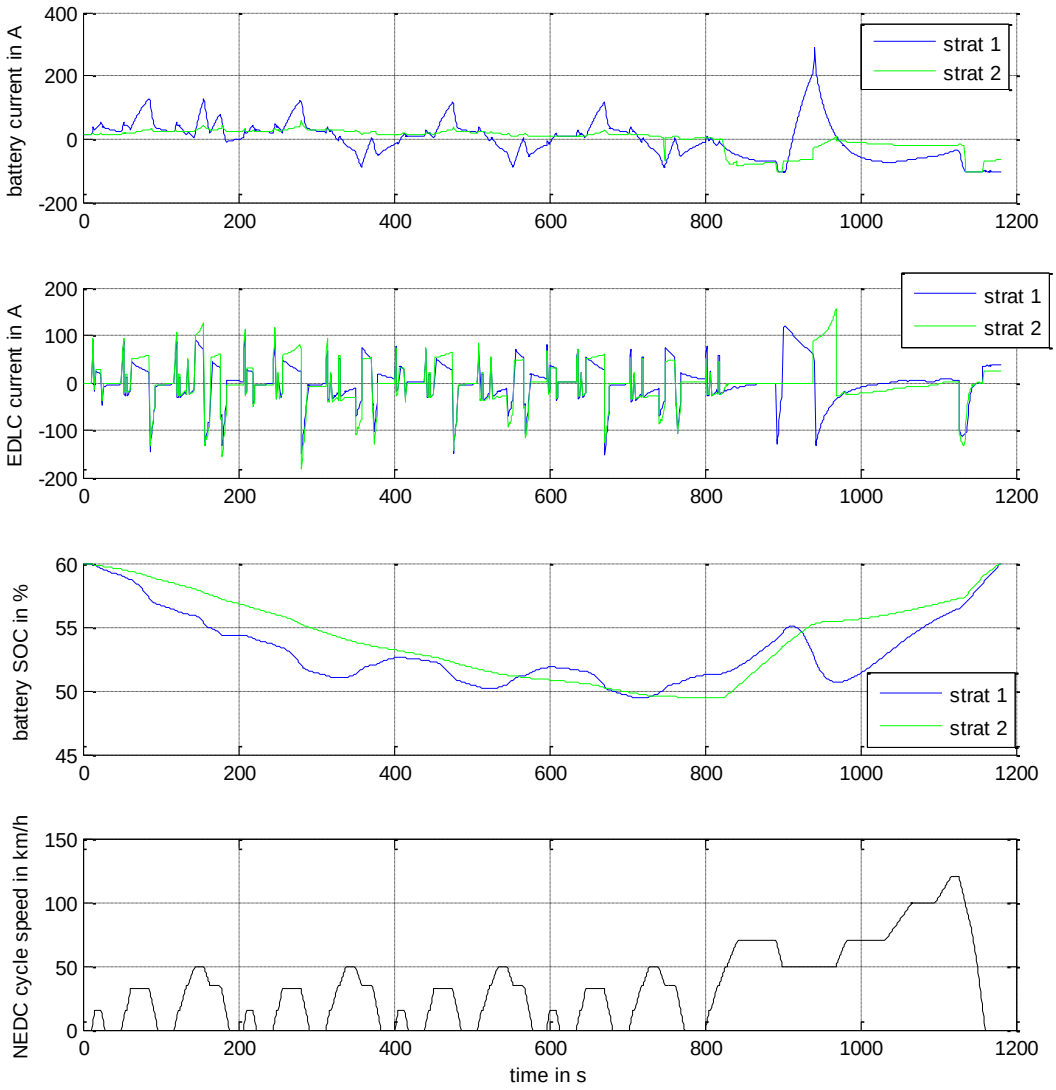

Fig. 20: Battery and EDLC current and battery SOC on NEDC cycle, rule-based method

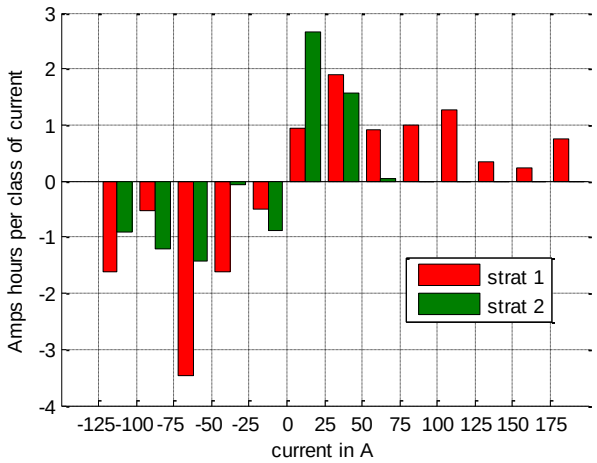

Fig. 21: Battery current solicitation on NEDC cycle, rule-based method

Fig. 23 and Fig. 24 show the SOC and the battery current stress for the NEDC using optimal control with the two different control objectives:

- Strat opt 1: objective is to minimize fuel consumption (K_{ibatt}=0),
- Strat opt 2: objective is a weighted function of consumption and battery current (K_{ibatt} =0.25).

These two strategies are meant to correspond to Strat 1 and Strat 2 with the rule-based method while using optimal control theory.

Looking at Fig. 23, it can be seen that introducing a weighting factor of battery current in the objective function results in a very different strategy for short time windows as well as long time intervals. With Strat opt 2, high battery currents especially in the negative range, are drastically reduced and absorbed by the EDLC. At the same time, the maximum SOC variation is reduced from 5% with Strat opt 1 to 2% with Strat opt 2. In fact taking into account the battery RMS current (Strat opt 2) the time passed in pure electrical mode is reduced, from 490 s to 398 s.

In both cases the optimal control method uses a smaller SOC amplitude than the rule-based method, which operates with a SOC variation of 11%.

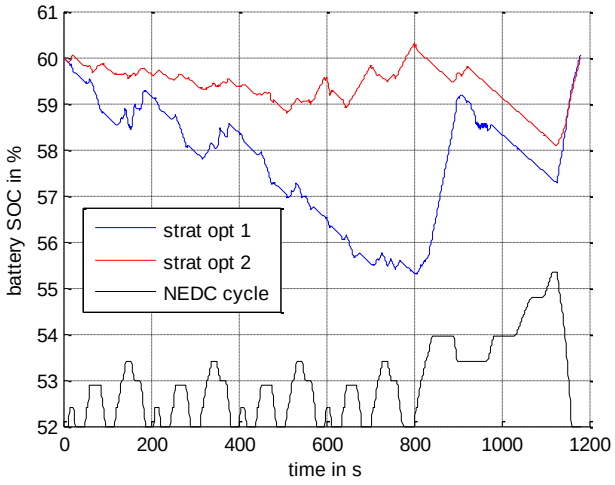

Fig. 22: Battery SOC on NEDC cycle, optimal control method

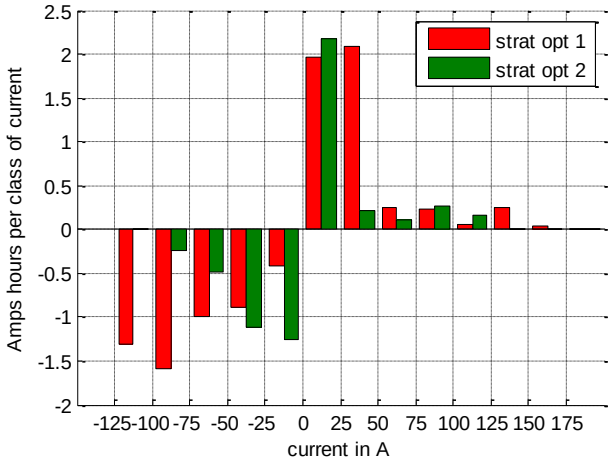

Fig. 23: Battery current solicitation on NEDC cycle, optimal control method

4.4.3.3. Validation of a rule-based method on realistic urban driving cycle

The parametric study (part 4.4.2) allows choosing sets of parameters which present the best trade-off between fuel consumption and battery current. However this set of parameters is determined on one cycle (NEDC in this case) and does not necessarily remain relevant for another driving cycle. A first validation is thus necessary using these sets of parameters to simulate an urban cycle and compare the results to optimal results and the parametric study performed on the NEDC cycle.

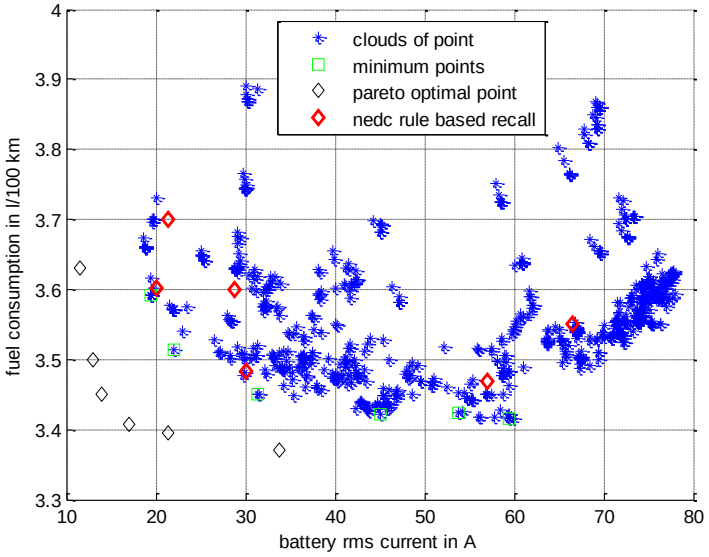

Fig. 24: Validation of rule-based method

Fig. 25 shows a comparison on urban driving cycle of the optimal method and the rule-based method:

- Black diamond shaped points are the Pareto optimal front obtained by the optimal presented method
- Blue stars represent the points obtained making a parametric study (cf part 4.4.2) on urban cycle using the rule-based control
- Green squares are some of the best points obtained in the parametric study
- Red diamonds are the points obtained using the sets of parameters corresponding to some best point of parametric study performed on NEDC cycle (Fig. 20 and Table 4).

It clearly appears that the sets of parameters determined on NEDC cycle remain globally relevant on urban driving cycles. An over fuel consumption of 2% is observed for the worst set of parameters. It is also observed that the rule-based method presents good performances for this driving cycle too (fuel consumption 3% higher compared to optimal points).

This tends to show that this rule-based method may be relevant to unseen realistic driving cycle.

5. Conclusion

In this paper energy management strategies of a hybrid vehicle with hybrid storage system were discussed. First the application of the Pontryagin's Minimum Principle for such an architecture was presented. Then a rule-based method, easily applicable on-line, is proposed and compared to the off-line optimal method.

The Pontryagin's Minimum Principle was applied to the problem considering two state variables. As a result we identified the Pareto optimal front between the two objectives: fuel consumption and battery RMS current. The utilized model implements look-up tables to simulate the electrical machine losses and fuel consumption. Therefore a non-analytical method has to be applied to find the Hamiltonian minimum.

A rule-based method, using two control levels, is proposed. A load-following charge-sustaining strategy, usually applied in parallel hybrid vehicles, is coupled with a low-pass first-order filter approach. This filtering step identifies the split of power between the battery and EDLC. To achieve an efficient control with the rule-based method, an iterative study has been performed to choose the more appropriate values of the parameters. Once tuned, this strategy shows overall good performances compared to the optimal control law (2-3 % higher fuel consumption). The results show high potential to reduce the battery RMS current using EDLC.

Moreover this study shows the importance of taking into account Pareto optimality (fuel consumption versus battery current) and not to minimize for fuel consumption only. In fact the Pareto front is relatively flat in the minimum fuel consumption area. Thus a good compromise may be found when increasing fuel consumption by a small amount while significantly decreasing the battery RMS current and thus probably the battery ageing.

Continuing this work, three main areas will be explored in the future:

- Performing experiment on real vehicle or HIL test bench.
- Extension of results to other representative driving cycles
- Implementation online of Pontryagin's Minimum Principle with estimation in real time of the Lagrange multipliers.

Original paper published in : Energy Conversion and Management 76 (2013) 437–452
https://doi.org/10.1016/j.enconman.2013.07.065

Appendix:

Nomenclature

Battery	
P_{0batt}	Power of the ideal battery ; without any losses
P_{batt}	Power of the battery
E_{batt}	Energy stored in the battery
I_{batt}	Battery current
U_{0batt}	Battery open circuit voltage
U_{batt}	Battery voltage
R_{batt}	Battery resistance
SOC	State of charge
η_f	Faradic efficiency of the battery
electrical double-layer capacitor (EDLC)	
P_{0edlc}	Power of the ideal EDLC; without any losses
P_{edlc}	Power of the EDLC
E_{edlc}	Energy stored in the EDLC
I_{1edlc}	EDLC current
I_{edlc}	EDLC current after DC/DC
U_{0edlc}	EDLC open circuit voltage
U_{edlc}	EDLC voltage
R_{edlc}	EDLC main resistance
C	EDLC main capacity
R_x	EDLC parallel resistance
C_x	EDLC parallel capacity
τ_x	EDLC time constant $1/R_xC_x$
U_x	EDLC voltage on R_x
U_{x0}	EDLC initial voltage on R_x
I_{Cx}	Current in C_x capacity
$\eta_{DC/DC}$	DC/DC converter efficiency
Electrical Network	
P_{0elec}	Vector $[P_{0batt}\ P_{0edlc}]$
P_{elec}	Vector $[P_{batt}\ P_{edlc}]$
E_{elec}	Electrical stored energy; Vector $[E_{batt}\ E_{edlc}]$
I_{elec}	Vector $[I_{batt}\ I_{edlc}]$
U_0	Vector $[U_{0batt}\ U_{0edlc}]$

References:

[1] K.T. Chau, Y.S. Wong, “Overview of power management in hybrid electric vehicles”, Energy Conversion and Management 43 (2002), pp 1953-1968.

[2] CC. Chan, “The state of the art of electric and hybrid vehicles”, Proceedings of the IEEE, vol. 90, (Feb.2002), issue2, pp 247-275.

[3] T. Katrasnik, “Hybridization of powertrain and downsizing of IC engine – A way to reduce fuel consumption and pollutant emissions – Part 1”, Energy Conversion and Management 48 (2007), pp 1411-1423.

[4] P. Sharma, T.S. Bhatti, “A review on electrochemical double-layer capacitors”, Energy Conversion and Management 51 (2010), pp 2901-2912.

[5] N. Omar, M. Daowd, P. van des Bossche, O. Hegazy, J. Smekens, T. Coosemans and Joeri van Mierlo, “Rechargeable Energy Storage Systems for Plug-in Hybrid Electric Vehicles—Assessment of Electrical Characteristics ”, Energies (2012), vol. 5, pp 2952-2988.

[6] N. Omar, M. Daowd, P. van des Bossche, T. Coosemans and Joeri van Mierlo, “Electrical Double-Layer Capacitors in Hybrid Topoligies—Assessment and Evaluation of their Performance”, Energies (2012), vol. 5, pp 4533-4568.

[7] R.M. Schupbach, C.Balda, “The role of Ultracapacitors in an Energy Storage Unit for Vehicle Power Management”, IEEE Vehicular Technology Conference, Volume 5, Issue 6-9, Oct. 2003, pp 3236-3240.

[8] S.M. Lukic, S.G. Wirsingha, F. Rodriguez, J.Cao, A. Emadi, “Power Management of an Ultracapacitor/Battery Hybrid Energy Storage System in an HEV”, IEEE VPPC 2006, pp 1-6, 6-8 Sept 2006, Windsor-United Kingdon.

[9] A. di napoli, F. crescimbini, F. giulii capponi, L. solero, “Control strategy for multiple Input DC-DC Power Convertes Devoted to hybrid vehicle Propulsion Systems”, Proceeding of the IEEE International symposium on Industrial Electronics 2002, pp 1036-1041, Vol.3.

[10] V. Paladini, T. Donateo, A. de Risi, D. Laforgia, « Super-capacitors fuel-cell hybrid electric vehicle optimization and control strategy development », Energy Conversion and Management 48 (2007), pp 3001-3008.

[11] A. Coopera, J. Furakawab, L. Lamc, M. Kellawayd, "The UltraBattery—A new battery design for a new beginning in hybrid electric vehicle energy storage", Journal of Power Sources 188 (2009), pp. 642–649.

[12] N. Omar, J. Van Mierlo, B. Verbrugge, P. Van den Bossche, "Power and Life Enhancement of Battery-Electrical Double Layer Capacitor for Hybrid Electric and Charge-Depleting Plug-in Vehicle Applications", Electrochimica Acta (2008), doi:10.1016/j.electacta.2010.03.039.

[13] E.Schaltz, A. Khaligh, P.O. Rasmussen, "Influence of Battery/Ultracapacitor Energy-Storage Sizing on Battery Lifetime in a Fuel Cell Hybrid Electric Vehicle", IEEE Transactions on Vehicular Technology, Vol. 58, N°8, October 2009, pp 3882- 3891.

[14] A. Khaligh, Li. Zhihao, Battery, "Ultracapacitor, Fuel Cell, and Hybrid Energy Storage Systems for Electric, Hybrid Electric, Fuel Cell, and Plug-In Hybrid Electric Vehicles: State of the Art", IEEE Transactions on Vehicular Technology, Vol. 59, N°6, July 2010, pp 2806-2814.

[15] K. Cagatay Bayindir, M. Ali Gozukucuk, A. Teke, "A comprehensive overview of hybrid vehicle: Powertrain configurations, powertrain control techniques and electronic control units", Energy Conversion and Management 52 (20011), pp 1305-1313.

[16] R. Chandrasekaran, G. Sikha, B.N. POPOV, "Capacity fade analysis of a battery/super capacitor hybrid and a battery under pulse loads – full cell studies", Journal of Applied Electrochemistry (2005) 35:1005–1013.

[17] F. Savoye, Impact of periodic current pulses on the performance and the lifetime of Lithium-ion batteries and the consequences on its processing in vehicular applications. PhD Thesis, Claude Bernard University, 2012.

[18] J.Scordia, M.Desbois-Renaudin, R.Trigui, B.Jeanneret and F.Badin, "Global Optimisation of Energy Management Laws in Hybrid Vehicles Using Dynamic Programming". I.J.Vehicle Design, Vol.39, No.4, 2005,pp 349-367.

[19] S. Delprat, J. Lauber, T.M. Guerra, J. Rimaux, Control of a parallel hybrid powertrain: optimal control, IEEE Transactions on Vehicular Technology, 53 (3), pp. 872-881, 2004.

[20] E. Vinot, R.Trigui, B.Jeanneret, J. Scordia, F. Badin, HEVs Comparison and Components Sizing Using Dynamic Programming, IEEE VPPC 07, Arlington, Texas

[21] C.R. Akli, X.Roboam, B.Sareni, A.Jeunesse, "Energy management and sizing of a hybrid locomotive", European conference on power electronic and application 2007, pp1-10, Sept. 2007, Aalborg-Danish.

[22] A.C. Baisden, A. Emadi, "Advisor-Based Model of a Battery and an Ultra-capacitor Energy Source for Hybrid Electric Vehicles", IEEE Transactions on Vehicular Technology, Vol. 53, N°1, January 2004,pp 199-205.

[23]M.A. Hannan, F.A. Azidin, A. Mohamed, "Multi-sources model and control algorithm of an energy management system for light electric vehicles", Energy Conversion and Management 62 (2012), pp 123-130.

[24] K. B. Wipke, M. R. Cuddy, and S. D. Burch, ADVISOR 2.1: "A User-Friendly Advanced Powertrain Simulation Using a Combined Backward/Forward Approach", IEEE Transactions on Vehicular Technology, 48, Issue 6, Nov 1999, pp 1751 – 1761

[25] E. Vinot, J.Scordia, R.Trigui, B.Jeanneret, F.Badin "Model simulation, validation and case study of the 2004 THS of Toyota Prius", Int.J. Vehicle Systems Modelling and Testing, Vol.3, No.3, 2008, pp 130-167.

[26] Y. Cheng, K. Chen, CC.Chan, A. Bouscayrol and S. Cui, "Global Modeling and Control Strategy Simulation for a Hybrid Electric Vehicle using Electrical Variable Transmission", IEEE VPPC 2008, 3-5 Sept 2008, Harbin-China.

[27] D.E. KirK, "Optimal Control Theory, An Introduction", Dover Publications, Inc. ISBN : 0486434842.

[28] P. Borne, G. Dauphin-Tanguy, J.P. Richard, F. Rotella, and I. Zambettakis, « Commande et optimisation des processus », Editions Technip 1990,ISBN : 2710805995.

[29] J-C Culioli, Introduction à l'optimisation, editor : ellipses, ISBN : 2729894284.

[30] K. Namwook, C. Sukwon, H. Peng , "Optimal control of hybrid vehicle based on Pontryagin's minimum principle", IEEE Transaction on control systems technology, vol. 19, N°5, September 2011, pp 1279-1287.

[31] S. Rimaux,M. Delhom, and E. Combes, "Hybrid vehicle powertrain: modelling and control", EVS 16, 1999.

[32] S. Kermani, S. Delprat, R. Trigui, T.M. Guerra, "Real time control of hybrid vehicle on a prescribed road", 17th World congress, the international federation of automatic, Seoul Korea July 6-11, 2008.

[33]S. Kermani, S. Delprat, T.M Guerra, R. Trigui., "Predictive energy management of hybrid vehicle", IEEE VPPC 08, Harbin, China.

[34] J. Bernard, S. Delprat, T.M. Guerra, F. Buecchi "Fuel Cell hybrid Vehicles: Global optimisation based on optimal control theory", International Review of Electrical Engineering, vol. 1, 2006, pp 352-362.

[35] H. Farzanehfard, D.Shekari Beyragh, E.Adib, "A Bidirectional soft switched ultracapacitor interface circuit for hybrid electric vehicles", Energy Conversion and Management 49 (2012), pp 3578-3584.

[36] A.L Allegre, A. Bouscayrol, R. Trigui, "Influence of control strategies on battery/supercapacitor hybrid Energy Storage Systems for traction applications", IEEE VPPC 09, (Dearborn) Michigan - September 2009.

[37] V.H. Johnson, "Battery performances models in Advisor", Journal of Power Sources 110 (2002), pp. 321-329.

[38] A.Guigue, M. Ahmadi, R.langlois, J.Hayes, « Pareto Optimality and Multiobjective Trajectory Planning for 7-DOF Redundant Manipulator", IEEE Transaction on Robotics, Vol. 26, Issue 6, pp 1094-1099, December 2010.

[39] Y. Sawaragi, H. Nakayama, and T. Tanino, "Theory of Multiobjective Optimization". Academic Press, Inc., Orlando, FL, 1985.

[40] M. Ecker, J. B. Gerschler, J. Vogel, S. Käbitz, F. Hust, P. Dechent, D. Uwe Sauer, "Development of a lifetime prediction model for lithium-ion batteries based on extended accelerated aging test data", Journal of Power Sources 215, pp 248-257, 2012.

[41] M. Montaru, S. Pellissier, “Frequency and Temporal Identification of Li-ion Polymer Battery Model Using Fractional Impedance” , Oil & Gas Science and Technology- Rev IFP, Vol. 65, N°1, 2010, pp 67-78.

[42] M. Einhorn, V. Conte, C. Kral et al., “Comparison of electrical battery models using a numerically optimized parameterization method”, IEEE Vehicle Power and Propulsion Conference, 2011, pp 1-7.

[43] X. Hu, S. Li, P. Huei, “A comparative study of equivalent circuit models for Li-ion batteries”, Journal of Power Sources, Vol. 198, 2012, pp 359-367.

[44] Lisheng Shi. and M. L. Crow, “Comparison of Ultra-capacitor Electric Circuit Models”, IEEE Power and Energy General Meeting, July 2008.

[45] B. Jeanneret, R. Trigui, F. Badin, F. Harel, “New Hybrid concept simulation tools, evaluation on the Toyota Prius car, 16th international electric vehicle symposium, Beijing”, China, October 13-16, 1999.

[46] R. Trigui, M. Desbois-Renaudin, B. Jeanneret, F. Badin, “Global Forward-Backward Approach for a Systematic Analysis and Implementation”, EET2004, march 18-20 th 2004, Estoril, Portugal.

[47] Mild Hybrid Project, funding by Valeo, 2001-2007. IFSTTAR 0725 report.

[48] R. Trigui, B.Jeanneret, B. Malaquin, C. Plasse, “Performance Comparison of Three Storage Systems for Mild HEVs Using PHIL Simulation”, IEEE Transactions on Vehicular Technology, Vol. 58, N°8, October 2009,pp 3959-3969.